ADVANCED ENERGY MATERIALS
www.advenergymat.de

The Redox-Mediated Nickel–Metal Hydride Flow Battery

*Teresa Páez, FeiFei Zhang, Miguel Ángel Muñoz, Lara Lubian, Shibo Xi, Roberto Sanz, Qing Wang, Jesús Palma, and Edgar Ventosa**

Each battery technology possesses intrinsic advantages and disadvantages, e.g., nickel–metal hydride (MH) batteries offer relatively high specific energy and power as well as safety, making them the power of choice for hybrid electric vehicles, whereas aqueous organic flow batteries (AORFBs) offer sustainability, simple replacement of their active materials and independent scalability of energy and power, making them very attractive for stationary energy storage. Herein, a new battery technology that merges the above mentioned battery technologies through the use of redox-mediated reactions is proposed that intrinsically possesses the main features of each separate technology, e.g., high energy density of the solid active materials, easy recyclability, and independent scalability of energy and power. To achieve this, $Ni(OH)_2$ and MHs are confined in the positive and negative reservoirs of an AORFB that employs alkaline solutions of potassium ferrocyanide and a mixture of 2,6-dihydroxyanthraquinone and 7,8-dihydroxyphenazine-2-sulfonic acid as catholyte and anolyte, respectively. An energy density of 128 Wh L^{-1} is achieved based on the capacity of the reservoirs leaving ample room for improvement up to the theoretical limit of 378 Wh L^{-1}. This new battery technology opens up new market opportunities never before envisaged, for redox flow batteries, e.g., domestic energy storage and heavy-duty vehicle transportation.

1. Introduction

Energy storage systems (ESSs) have become essential elements in our modern society. Among the various EESs, batteries have experienced a rapid growth driven by the expanding market of portable electronics, implementation of energy from renewable sources, electrification of transportation, and other emerging technologies.[1] There are several battery technologies in the market, and more are under development at lab scale to fulfill the growing requirements of applications. In general, battery technologies can be categorized into two main groups according to the location of the energy storing materials (active materials): redox flow batteries and static batteries. In the former, active materials are stored outside the electrochemical reactor, while in the latter, they are located inside the battery cell. Each group possesses intrinsic advantages and disadvantages. While redox flow batteries offer independent scalability of energy and power, and easy recyclability, static batteries usually have higher energy densities. As a result, static batteries are used in applications demanding higher energy densities, whereas redox flow batteries are more suitable for stationary energy storage.

The development of a battery technology combining the best features of each category has been long desired. The use of solid electroactive materials stored in the external reservoirs of redox flow batteries is the most direct approach; however, challenging to be realized. The semisolid flow battery, in which dense but flowable slurries of solid materials are used, has demonstrated a drastic increase in energy density.[2,3] However, the practical application of this concept raised concerns as viscous slurries containing solid particles must be continuously flown through the system. This main concern is overcome by the confinement of the solid electroactive materials in the external reservoirs. In this case, the dissolved electroactive species act as

T. Páez, J. Palma
IMDEA Energy
Avda. Ramón de la Sagra 3, Móstoles, Madrid E-28935, Spain
T. Páez
Departamento de Ingeniería Química Industrial y del Medio Ambiente
Escuela Técnica, Superior de Ingenieros Industriales
Universidad Politécnica de Madrid
C/José Gutierrez Abascal, 2, Madrid E-28006, Spain

The ORCID identification number(s) for the author(s) of this article can be found under https://doi.org/10.1002/aenm.202102866.

DOI: 10.1002/aenm.202102866

F. Zhang, Q. Wang
Department of Materials Science and Engineering
Faculty of Engineering
National University of Singapore
Singapore 117576, Singapore
M. Á. Muñoz, L. Lubian, R. Sanz, E. Ventosa
Department of Chemistry
University of Burgos
Pza. Misael Bañuelos s/n, Burgos E-09001, Spain
E-mail: eventosa@ubu.es
L. Lubian, E. Ventosa
International Research Centre in Critical Raw Materials—ICCRAM
University of Burgos
Plaza Misael Bañuelos S/n, Burgos E-09001, Spain
S. Xi
Institute of Chemical and Engineering Sciences
A*STAR
Singapore 627833, Singapore

molecular wires (redox mediators) transferring charges between the electrochemical reactor and the solid materials confined in the reservoirs, and enabling the decoupling of energy and power. The use of solid electroactive materials boosts the energy density with respect to conventional redox flow batteries. In early attempts, nonaqueous electrolytes were employed,[4–6] and then extended to aqueous chemistries,[7–10] due to a higher practical interest of the latter. Despite the great promise of solid redox-mediated flow batteries (also referred to as solid targeting or solid booster), only a couple of examples of aqueous full battery using solid materials in both compartments have been realized.[11,12]

Herein, we report the fundamentals and proof of concept of a high-energy alkaline full redox-mediated flow battery based on the successful combination of two established battery technologies through the use of redox-mediating processes, i.e., static Ni–MH battery and aqueous organic redox flow battery (AORFB), into a new battery technology: the redox-mediated nickel–metal hydride (MH) flow battery. This novel flow battery combines the high energy density of Ni–MH solid materials with the easy recyclability and independent scalability of energy and power of flow configuration. The proof of concept in this work opens up new directions in the field of energy storage that will require contributions from different disciplines.

2. Results and Discussion

2.1. The Concept of Redox-Mediated Nickel–Metal Hydride Flow Battery

The Ni–MH battery is a safe and mature technology that possesses relatively high energy density (>300 Wh L^{-1} at the material level) and long cycle life if depth of discharge (DoD) is controlled (20 000 cycles for a DoD of 50%).[13] Therefore, $Ni(OH)_2$ and MHs are reliable and suitable solid electroactive materials to boost the energy density of a redox-mediated flow battery. The resulting battery technology would enable independent scalability of energy and power of the Ni–MH battery chemistry, e.g., adjusted for 8 h energy storage cycles, and facilitate enormously the recyclability by simple replacement of solid materials in the accessible external reservoirs. **Figure 1** illustrates the working principle of the proposed redox-mediated Ni–MH flow battery. $Ni(OH)_2$ and MH solid electroactive materials (boosters) are confined in the reservoirs of the positive and negative compartments, respectively. Among the various examples of promising organic electroactive species proposed in organic aqueous flow batteries,[14–18] our flow battery employs alkaline electrolyte solutions containing potassium ferrocyanide and a mixture of 2,6-dihydroxyanthraquinone (DHAQ) and 7,8-dihydroxyphenazine-2-sulfonic acid (DHPS) as redox mediators in the positive and negative sides, respectively. Indeed, to illustrate that our approach combines the best of the two battery technologies, dissolved compounds previously reported as energy storage species in conventional redox flow batteries, i.e., $K_4[Fe(CN)]_6$, DHAQ, and DHPS, were selected as redox mediators,[19,20] while $Ni(OH)_2$ and MH ($LaNi_5$-type) materials were directly extracted from commercial Ni–MH batteries (Panasonic HHR-110AA).

The key aspect in a redox-mediated flow battery is the spontaneous and reversible charge-transfer reactions between the redox electrolyte (mediator) and the solid electroactive material (solid booster) that occur in the external reservoirs. To achieve this, the redox potential of the electrolyte must be above and below that of the solid material during the charge and discharge processes, respectively, for the positive compartment. As shown in our previous work,[21] as the redox potential of ferrocyanide in 1 M KOH is very close to that of $Ni(OH)_2$, an

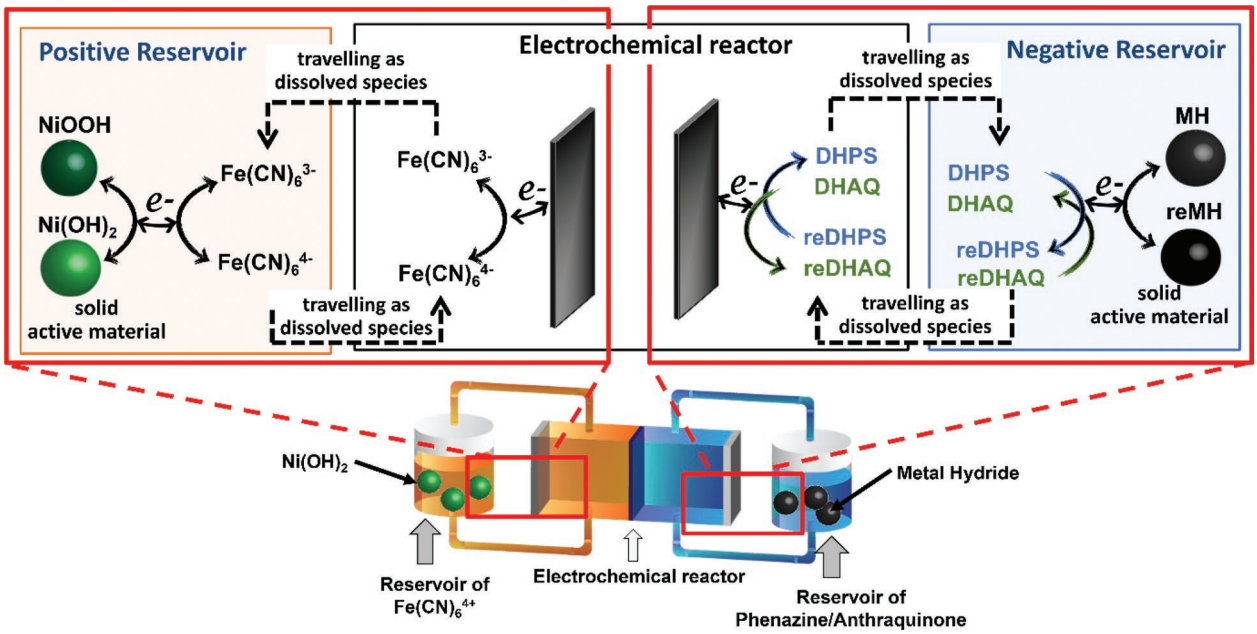

Figure 1. Schematic illustration of the working principle of the proposed redox-mediated Ni–MH flow battery, in which the dissolved active species in positive (ferrocyanide) and negative compartments (DHPS and DHAQ) not only store energy but also act as redox mediators to enable reversible charge storage in high-energy solid active material boosters ($Ni(OH)_2$ and MHs) confined in the reservoir.

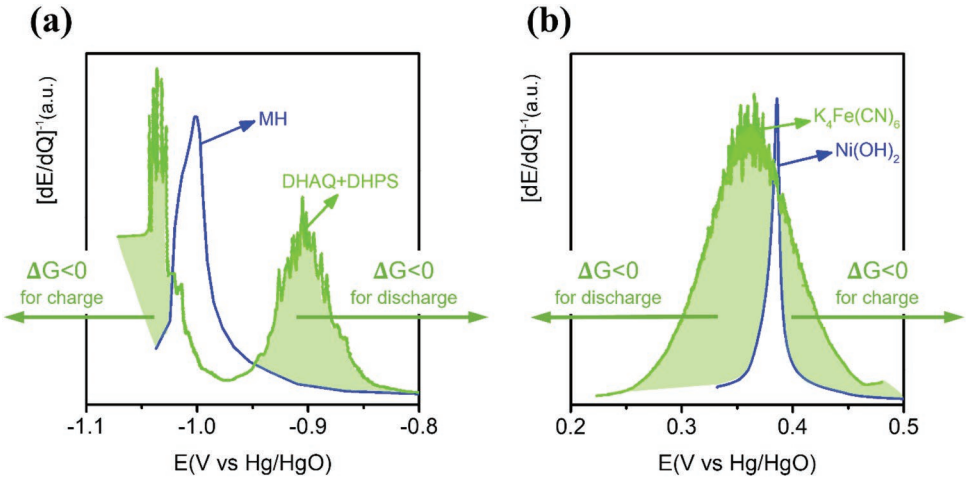

Figure 2. Differential potential plot (inverse of time derivative of *E* against potential) recorded at open-circuit potential during galvanostatic intermittent titration technique (GITT) measurements, revealing the redox potential at equilibrium: a) an electrolyte containing 0.2 M DHAQ + 0.2 M DHPS and a conventional MH electrode, and b) an electrolyte containing 0.3 M K4[Fe(CN)]$_6$ and a conventional Ni(OH)$_2$ electrode.

electrolyte solution containing ferrocyanide in 1 M KOH acts as a single Nernstian mediator for both the charge and discharge processes of Ni(OH)$_2$ solid particles. Figure S3a,b (Supporting Information) represents the thermodynamic driving forces for the spontaneous and reversible reactions. In the case of the negative compartment, the redox potential of the electrolyte must be below and above that of the solid material during the charge and discharge processes, respectively. It should be noted that the charge process in the negative compartment implies reduction of the solid material. We did not find any single redox mediator, which is able to mediate both the charge and discharge processes of MH, as the redox potential of none of the investigated species completely matches up the redox potential of the MH. As an alternative for this proof-of-concept study, the combination of two redox mediators was used in the negative compartment. Figure S3c,d (Supporting Information) shows the thermodynamic driving forces for the charge and discharge processes, respectively, in the negative compartment when using two redox mediators. The driving forces for charge transfer increase through the use of two mediators, while the voltage efficiency is penalized (larger difference between charge and discharge potentials). For our system, **Figure 2** shows the differential potential at open circuit versus the potential of the selected redox mediators and solid material boosters. It should be noted that the comparison of cyclic voltammetry (CV) can be misleading to evaluate thermodynamic aspects since CVs are not recorded at equilibrium. The curve of the ferrocyanide solution completely covers that of the Ni(OH)$_2$ (Figure 2b), indicating that the dissolved ferrocyanide can act as a single redox mediator. In the case of the negative compartment (Figure 2a), the curves of DHPS and DHAQ are below and above that of the MH, revealing that dissolved DHPS and DHAQ can act as redox mediators for the charge and discharge of MH, respectively.

2.2. Redox-Mediated Reaction between Anolyte and MHs

A testing flow cell (**Figure 3**a), in which the positive compartment was largely oversized, was used to quantify the practical utilization rate of MHs. Figure 3b shows the evolution of the storage capacity with cycles in the absence and presence of MHs confined in the external reservoir. The cell containing 5 g of MHs delivered 850 mAh exhibiting a cycling stability (10 cycles for 100 h) as good as that of the cell cycled without MHs. In the absence of MH particles, electrolyte containing 0.2 M DHAQ and 0.2 M DHPS stored 247 mAh, which was very close to its maximum theoretical value of 278 mAh. As the amount of solid material confined in the reservoir is known, the charge storage capacity in MHs is calculated as the difference between the capacity in the absence and in the presence of solid material divided by the mass of MHs. Figure 3c displays the experimental values of storage capacity of MHs as a function of its mass loading (amount of solid per total volume (electrolyte + solid)) obtained at a current density of 20 mA cm^{-2}. In all cases, the storage capacity in MHs (extra binder and carbon black are not included to evaluate the intrinsic value of MH) was ≈120 mAh g^{-1}. Considering that a commercial battery of 1180 mAh (Panasonic HHR-110AA) contains 7.2 g of MH (165 mAh g_{MH}^{-1}), an MH utilization rate of 73% was achieved using a combination of DHAQ and DHPS as redox mediators. Thus, the use of two redox mediators enables a very high utilization rate at a reasonable current density, but it also leads to poorer voltage efficiency (80% at 20 mA cm^{-2} in this case) as shown in the voltage profile (Figure 3d). The higher-voltage plateau is extended during the charge process since DHPS is the active mediator during this process, while the lower-voltage plateau is extended during the discharge process as DHAQ acts as a mediator for this process.

The redox-mediating process between the redox electrolyte and the confined solid materials was confirmed by ex situ X-ray absorption spectra (XAS) measurement (**Figure 4**), as reversible hydrogenation/dehydrogenation of MH particles that were confined in the external reservoir was observed. Pristine MH (LaNi$_5$-type) materials were directly extracted from commercial Ni–MH batteries. The charged and discharged MH samples were collected from the negative tank at fully charged and discharged states sequentially, sealed in a plastic bag with some

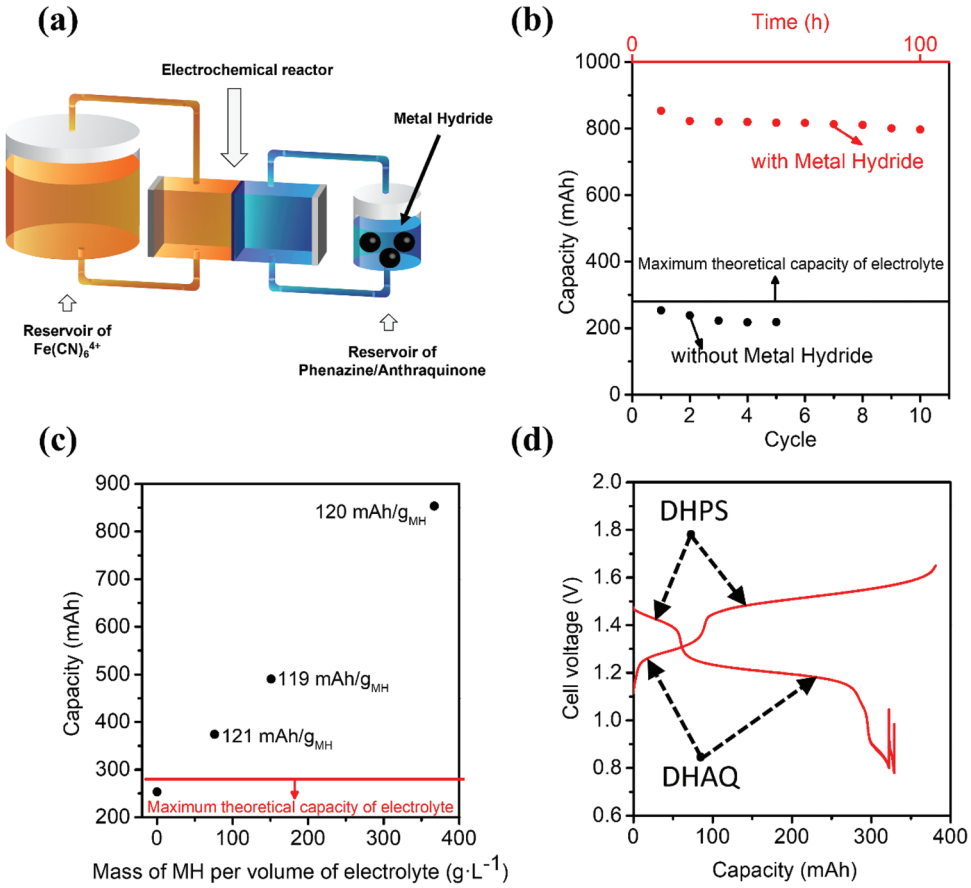

Figure 3. Electrochemical performance of a redox flow battery containing a large excess of $K_4[Fe(CN)]_6$ electrolyte in the positive compartment and a mixture of DHPS and DHAQ electrolyte plus confined MH in the negative compartment. a) Scheme of the cell. b) Evolution of the capacity with cycles at ±20 mA cm^{-2} for 13 mL of 0.2 M DHAQ and 0.2 M DHPS in 1.5 M KOH in the absence of MH (maximum capacity of electrolyte of 278 mAh) and in the presence of 5 g of MHs. c) Evolution of the reversible charge stored as a function of the mass of MH added to the electrolyte (g_{solid} $L_{electrolyte}^{-1}$). In all cases, the utilization rate in half-cell is close to 73%. d) Voltage profile of a cell containing MH.

electrolyte under N_2 protection and detected immediately. The edge X-ray absorption near edge structure (XANES) and extended X-ray absorption fine structure (EXAFS) of the Ni *K*-edge were performed at the X-ray absorption fine structure for catalysis beamline of the SSLS. Figure 4a shows Ni *K*-edge XANES spectra for pristine, charged, and discharged MHs. The decrease in area at the edge (shaded area) after charging is partly in response to the large lattice expansion after hydrogenation,

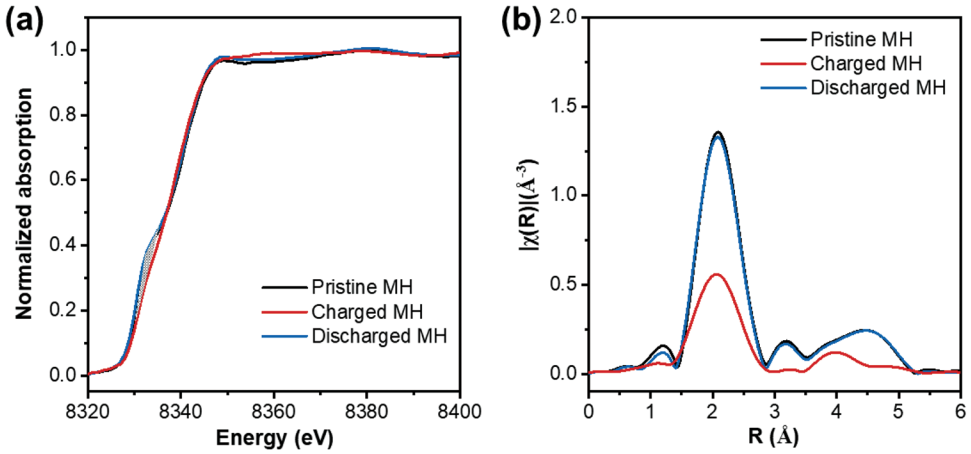

Figure 4. Ex situ X-ray absorption spectra (XAS) characterization of MHs: a) nickel *K*-edge XANES spectra and b) Fourier-transformed EXAFS spectra of pristine, charged, and discharged MHs.

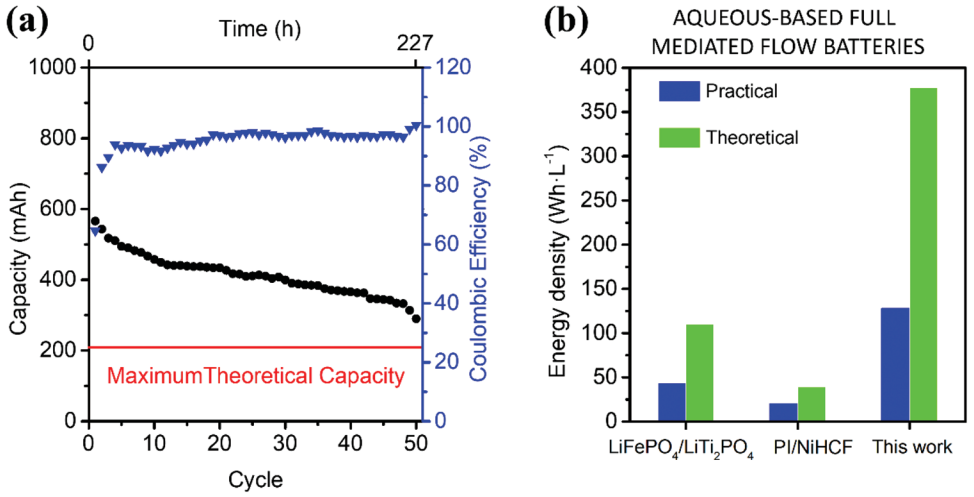

Figure 5. a) Electrochemical performance of a redox-mediated Ni–MH flow battery. Evolution of the capacity and Coulombic efficiency versus number of cycles at ±20 mA cm^{-2} for 26 mL of 0.3 M $K_4Fe(CN)_6$ in 1.5 M KOH and 134 $g_{Ni(OH)2}$ $L_{catholyte}^{-1}$ (3.5 g of $Ni(OH)_2$) and 13 mL of 0.2 M DHAQ + 0.2 M DHPS in 1.5 M KOH and 154 g_{MH} $L_{anolyte}^{-1}$ (2 g of MH). Maximum capacity of electrolyte of 209 mAh. b) Representation of the theoretical and achieved energy density. Values of $LiFePO_4/LiTi_2PO_4$ and PI/NiHCF are obtained from refs. [11] and [12].

which is identical to those observed by Suenobu et al. for $LaNi_5$ powder before and after hydrogenation.[22] Figure 4b shows the magnitudes of the Fourier-transformed EXAFS data of these samples obtained by the Fourier analysis. A most strong peak appeared on the Ni edge at about 2 Å, corresponding to mainly Ni–Ni and partially Ni–La distances. The decrease of this main peak height after charging is attributed to either decreasing of the coordination number or increasing of the static disorder induced by hydrogen. It indicates the chemical hydrogenation of MH particles by reduced mediators. Furthermore, both XANES and EXAFS spectra of the discharged MH sample changed back to that of pristine one, suggesting the reversible hydrogenation/dehydrogenation of MH particles in the external reservoir during the charge and discharge processes.

2.3. Mediated Ni–MH Full Flow Battery

As a proof of concept of the full Ni–MH flow battery, 3.5 g of $Ni(OH)_2$ and 2 g of MH were confined in the positive and negative reservoirs of a DHAQ+DHPS//$K_4[Fe(CN)_6]$ flow battery. **Figure 5**a shows the evolution of capacity with cycles of this full cell cycled at 20 mA cm^{-2}. For an operating period of 126 h (between cycles 10 and 40), a steady capacity retention of 99.84% h^{-1} (99.33% per cycle) was observed. Nevertheless, the capacity decay is not related to the use of solid electroactive material, but it appears to be associated with the partial incompatibility of anthraquinone and phenazine. Figure S4a (Supporting Information) shows an excellent and stable cycling stability for both independent DHAQ//$K_4[Fe(CN)_6]$ and DHPS//$K_4[Fe(CN)_6]$ cells while the capacity decay is observed for the cell with the mixture of DHAQ+DHPS as anolyte. The resulting capacity retention for the DHAQ+DHPS//$K_4[Fe(CN)_6]$ cell is 99.62% h^{-1}, leading to a capacity fading rate in the absence of solid booster (0.38% h^{-1}) as twice as high as that recorded for the mediated flow battery (0.18% h^{-1}). Although the anolyte "only" contributes with 20 Ah L^{-1} to the volumetric capacity, the disappearance of redox mediator and the appearance of decomposition products are highly probably influencing negatively the redox-mediating process. Enhancing the cyclability of the redox-mediating electrolyte is of key importance for improving the cycle stability of the redox-mediated battery. Thus, we explored the possibility of using two redox mediators based on the same core structure (phenazine derivatives). The redox potentials of 2-hydroxy phenazine (HP) and DHPS make them suitable redox mediators for MHs. Unfortunately, the cycle stability of an anolyte containing both HP and DHPS did not result in any improvement in cycle stability. Indeed, the stability decreased with respect to that of DHAQ+DHPS (Figure S4b, Supporting Information). Currently, our efforts are focused on finding a single redox mediator for MHs to enhance the cycle stability. It should be noted that water electrolysis during the charge process was likely occurring based on the values of Coulombic efficiency (CE), which is likely due to the combination of three aspects: I) the large operating voltage (second voltage plateau is at 1.45–1.50 V), II) the mild alkaline media, and III) the relatively low current density. Thus, CE can be improved by employing a redox mediator with a slightly higher (more anodic) redox potential, by optimizing the pH of the electrolyte and by operating at higher current densities. Importantly, Figure 5a shows that this cell achieved a practical charge capacity (580 mAh) largely exceeded the theoretical limit of the electrolyte (209 mAh). This corresponds to a utilization rate of 42% (106 mAh g^{-1}) and 90% (151 mAh g^{-1}) for $Ni(OH)_2$ and MHs, respectively, when operated at ±20 mA cm^{-2}. Note that the utilization rate of MH increased from half-cell configuration (73%) to full-cell configuration (90%), which is attributed to i) longer cycles and ii) constant pH in full cell during cycling: in half-cell, MHs take H^+ while ferrocyanide releases K^+ during the charge process (slightly change the pH), while NiOOH uptakes OH^- in full cell. To quantitatively benchmark the results achieved in this work against the state-of-the-art for redox-mediated flow batteries, the energy density of our system was estimated neglecting the volume of electrolyte in the tubes,

Table 1. Values achieved in this work.

	C_{solid} [Ah L^{-1}]	$C_{electrolyte}$ [Ah L^{-1}]	α [0–1]	β [0–1]	$C_{reservoir}$ [Ah L^{-1}]
Positive tank	1180	8	0.42	0.59	208
Negative tank	1300	21	0.90	0.83	216

reactor, etc., which is reasonable upon upscaling. To do this, Equation (1) was followed,[4,10–12] in which storage capacity of the reservoir ($C_{reservoir}$) can be estimated based on the capacity of solids (C_{solid}), capacity of electrolyte ($C_{electrolyte}$), utilization rate (α), and packing porosity of the solid material (β)

$$C_{reservoir} = \alpha(1-\beta)C_{solid} + \beta C_{electrolyte} \quad (1)$$

Tables 1 and **2** summarize the practical values achieved in this work and the theoretical limits for this battery chemistry, respectively. These values result in an energy density of 128 Wh L^{-1} having a maximum theoretical value of 378 Wh L^{-1}. Figure 5b compares the values of energy density with the state-of-the-art values for full redox-mediated flow batteries calculated using the same methodology clearly revealing the great potential of the battery chemistry proposed in this work.

The use of redox mediators is beneficial not only for boosting energy density but also for widening the temperature range of operation, as discussed by Wang and co-workers.[10] In our case, 0.3 M ferrocyanide electrolyte does not precipitate in the range from –10 and +70 °C, while 0.2 M DHAQ + 0.2 M DHPS is stable between –20 and +70 °C (Figure S5a, Supporting Information). Although the decrease in temperature led to higher internal resistance (as indicated by the separation between charge and discharge plateaus) resulting in lower storage capacity at 20 mA cm^{-2}, the redox-mediated Ni–MH flow battery was able to operate and exceed the theoretical capacity of the electrolyte in the range between –10 and +60 °C (Figure S5b, Supporting Information).

3. Conclusions

The proof of concept of the redox-mediated Ni–MH flow battery was demonstrated in this work. To achieve this, an electrolyte containing ferrocyanide was used as a single Nernstian redox mediator for solid $Ni(OH)_2$ particles confined in the positive compartment, while an electrolyte containing a mixture of DHAQ and DHPS was used as the redox mediator for solid MH material, achieving utilization rates of 42% (106 mAh g^{-1}) for the former and 90% (151 mAh g^{-1}) for the later at a current density of 20 mA cm^{-2} in full-cell configuration. A practical energy density of 128 Wh L^{-1} and a capacity retention of 99.33% per cycle and 99.84% h^{-1} were achieved. Provided the high volumetric capacity of $Ni(OH)_2$ and MHs (>1000 Ah L^{-1} based on bulk density), research efforts must now be focused on two critical aspects to push this technology forward. On the one hand, finding a suitable single Nernstian mediator for the negative compartment will enhance the cycle stability (incompatibility of two redox mediators) and voltage efficiency (voltage difference between the two redox mediators). On the other hand, the reactor design and fluid dynamics for the external reservoir will improve the packing of the solid materials maintaining high utilization rates that will boost the practical energy density considering the limits of 378 Wh L^{-1}.

Table 2. Theoretical values for the battery chemistry developed in this work.

	C_{solid} [Ah L^{-1}]	$C_{electrolyte}$ [Ah L^{-1}]	α [0–1]	β[a)] [0–1]	$C_{reservoir}$ [Ah L^{-1}]
Positive tank	1180	8	1	0.5	594
Negative tank	1300	21	1	0.5	660

[a)]Value demonstrated previously in ref. [23].

The integration of Ni–MH battery chemistry in a redox flow battery architecture results in a series of advantages, which are intrinsic from the flow battery configuration: i) independent scalability of power and energy, ii) easy access to the active materials for the state of health maintaining, and iii) simplified recyclability. Specific examples are as follows: i) the redox-mediated Ni–MH flow battery can adjust a power-to-energy ratio of 0.1, e.g., 1 kW of power while 10 kWh of energy, which is not possible for a conventional Ni–MH battery. ii) If the capacity of Ni electrode is fading, reducing the energy storage capacity of the battery, $Ni(OH)_2$ can be replaced independently. iii) At the end of life, battery does not need to be crushed to recover the materials of interest from spent electrodes since there is direct access. In addition to these general advantages of redox flow batteries, flow configuration is of great asset for the Ni–MH battery chemistry; the relatively low cell voltage and limited current density of conventional Ni–MH batteries result in a significant contribution of inactive elements of the cell (e.g., current collectors) to the specific energy. In our redox-mediated flow battery, the use of bipolar plates, higher current density (potentially >80 mA cm^{-2}), and an increase in power-to-energy ratio reduces considerably the contribution of inactive elements to the specific energy. Additionally, an increase in power-to-energy ratio further reduces the contribution of inactive materials. Due to its unique characteristics, new market opportunities will be potentially opened up for this new battery technology, which were not considered for redox flow batteries before, such as domestic energy storage, heavy-duty vehicles, and off-road transportation (e.g., railway).

4. Experimental Section

Materials: All chemicals were purchased from commercial suppliers and used without further purification. 2,5-Dihydroxy-1,4-benzoquinone, 3,4-diaminobenzenesulfonic acid, *p*-benzoquinone, and benzene-1,2-diamine were purchased from Fluorochem. Diethylether, ethyl acetate, and ethanol were purchased from Carlo Erba Reagents.

Preparation of Electrolytes: In the DHPS + DHAQ–MH//$K_4Fe(CN)_6$ flow cell, the anolyte was prepared by dissolving 0.7 g of DHPS and 0.6 g of DHAQ in 2.5 M KOH to afford 13 mL of 0.2 M DHPS, 0.2 M 2,6-DHAQ, and 1.5 M KOH. The catholyte was prepared by dissolving 33.2 g of potassium ferrocyanide in 1.5 M KOH to afford 300 mL of 0.3 M ferrocyanide. In the DHPS + DHAQ–MH//$K_4Fe(CN)_6$–$Ni(OH)_2$ flow cell, the anolyte was prepared by dissolving 0.7 g of DHPS and 0.6 g of DHAQ in 2.5 M KOH to afford 13 mL of 0.2 M DHPS, 0.2 M DHAQ, and 1.5 M KOH. The catholyte was prepared by dissolving 2.9 g of $K_4Fe(CN)_6$ in 1.5 M KOH to afford 300 mL of 0.3 M $K_4Fe(CN)_6$-.

Deionized water was used to prepare all electrolytes. In the case of anolytes, the solutions were purged with nitrogen prior to their use.

Flow Batteries: Filter-pressed flow cell using Nafion 212 and graphite felt as the ion selective membrane and electrodes were used in this study. The projected area of the cell was 9 cm^2. The flow rate was fixed at ≈50 mL min^{-1}.

Electrochemical Characterization: Galvanostatic charge–discharge measurements were conducted using a Biologic VMP multichannel potentiostat. The battery was galvanostatically charged at 20 mA cm^{-2} with a voltage limit of 1.7. Subsequently, it was discharged at a current density of –20 mA cm^{-2} with a voltage limit of 0.5 V.

Supporting Information

Supporting Information is available from the Wiley Online Library or from the author.

Acknowledgements

The authors acknowledge the financial support by the Spanish Government through the Research Challenges Programme (Grant No. RTI2018-099228-A-I00). E.V. thanks the MINECO for the financial support (RYC2018-026086-I). A spelling mistake in the author byline entry for Roberto Sanz was rectified on January 6, 2022.

Conflict of Interest

The authors declare no conflict of interest.

Data Availability Statement

The data that support the findings of this study are available from the corresponding author upon reasonable request.

Keywords

electrochemistry, redox flow batteries, redox mediators, redox targeting, solid boosters

Received: September 15, 2021
Revised: October 15, 2021
Published online: November 16, 2021

[1] P. Alotto, M. Guarnieri, F. Moro, *Renewable Sustainable Energy Rev.* **2014**, *29*, 325.
[2] M. Duduta, B. Ho, V. C. Wood, P. Limthongkul, V. E. Brunini, W. C. Carter, Y. M. Chiang, *Adv. Energy Mater.* **2011**, *1*, 511.
[3] Y. Yang, G. Zheng, Y. Cui, *Energy Environ. Sci.* **2013**, *6*, 1552.
[4] C. Jia, F. Pan, Y. G. Zhu, Q. Huang, L. Lu, Q. Wang, *Sci. Adv.* **2015**, *1*, https://doi.org/10.1126/sciadv.1500886.
[5] M. Zhou, Y. Chen, Q. Zhang, S. Xi, J. Yu, Y. Du, Y.-S. Hu, Q. Wang, *Adv. Energy Mater.* **2019**, *9*, 1901188.
[6] Y. G. Zhu, Y. Du, C. Jia, M. Zhou, L. Fan, X. Wang, Q. Wang, *J. Am. Chem. Soc.* **2017**, *139*, 6286.
[7] E. Zanzola, C. R. Dennison, A. Battistel, P. Peljo, H. Vrubel, V. Amstutz, H. H. Girault, *Electrochim. Acta* **2017**, *235*, 664.
[8] E. Zanzola, S. Gentil, G. Gschwend, D. Reynard, E. Smirnov, C. R. Dennison, H. H. Girault, P. Peljo, *Electrochim. Acta* **2019**, *321*, 134704.
[9] Y. Chen, M. Zhou, Y. Xia, X. Wang, Y. Liu, Y. Yao, H. Zhang, Y. Li, S. Lu, W. Qin, X. Wu, Q. Wang, *Joule* **2019**, *3*, 2255.
[10] Y. Cheng, X. Wang, S. Huang, W. Samarakoon, S. Xi, Y. Ji, H. Zhang, F. Zhang, Y. Du, Z. Feng, S. Adams, Q. Wang, *ACS Energy Lett.* **2019**, *4*, 3028.
[11] J. Yu, L. Fan, R. Yan, M. Zhou, Q. Wang, *ACS Energy Lett.* **2018**, *3*, 2314.
[12] M. Zhou, Y. Chen, M. Salla, H. Zhang, X. Wang, S. R. Mothe, Q. Wang, *Angew. Chem., Int. Ed.* **2020**, *59*, 14286.
[13] M. Brady, *Assessment of Battery Technology for Rail Propulsion Application*, Federal Railroad Administration, Washinghton, DC **2017**.
[14] R. Feng, X. Zhang, V. Murugesan, A. Hollas, Y. Chen, Y. Shao, E. Walter, N. P. N. Wellala, L. Yan, K. M. Rosso, W. Wang, *Science* **2021**, *372*, 836.
[15] J. Huang, S. Hu, X. Yuan, Z. Xiang, M. Huang, K. Wan, J. Piao, Z. Fu, Z. Liang, *Angew. Chem., Int. Ed.* **2021**, *60*, 20921.
[16] S. Hu, T. Li, M. Huang, J. Huang, W. Li, L. Wang, Z. Chen, Z. Fu, X. Li, Z. Liang, *Adv. Mater.* **2021**, *33*, 2005839.
[17] S. Hu, L. Wang, X. Yuan, Z. Xiang, M. Huang, P. Luo, Y. Liu, Z. Fu, Z. Liang, *Energy Mater. Adv.* **2021**, *2021*, https://doi.org/10.34133/2021/9795237.
[18] X. Li, P. Gao, Y.-Y. Lai, J. D. Bazak, A. Hollas, H.-Y. Lin, V. Murugesan, S. Zhang, C.-F. Cheng, W.-Y. Tung, Y.-T. Lai, R. Feng, J. Wang, C.-L. Wang, W. Wang, Y. Zhu, *Nat. Energy* **2021**, *6*, 873.
[19] K. Lin, Q. Chen, M. R. Gerhardt, L. Tong, S. B. Kim, L. Eisenach, A. W. Valle, D. Hardee, R. G. Gordon, M. J. Aziz, M. P. Marshak, *Science* **2015**, *349*, 1529.
[20] A. Hollas, X. Wei, V. Murugesan, Z. Nie, B. Li, D. Reed, J. Liu, V. Sprenkle, W. Wang, *Nat. Energy* **2018**, *3*, 508.
[21] T. Páez, A. Martínez-Cuezva, J. Palma, E. Ventosa, *ACS Appl. Energy Mater.* **2019**, *2*, 8328.
[22] T. Suenobu, H. Sakaguchi, T. Tsuji, H. Kanai, S. Yoshida, G. Adachi, *Bull. Chem. Soc. Jpn.* **2006**, *64*, 3522.
[23] M. Zhou, Q. Huang, T. N. Pham Truong, J. Ghilane, Y. G. Zhu, C. Jia, R. Yan, L. Fan, H. Randriamahazaka, Q. Wang, *Chem* **2017**, *3*, 1036.